Surface-acoustic-wave-driven ferromagnetic resonance in (Ga,Mn)(As,P) epilayers

L. Thevenard,[1,2,*] C. Gourdon,[1,2] J. Y. Prieur,[1,2] H. J. von Bardeleben,[1,2] S. Vincent,[1,2] L. Becerra,[1,2] L. Largeau,[3] and J.-Y. Duquesne[1,2]

[1]*CNRS, UMR7588, Institut des Nanosciences de Paris, 4 place Jussieu, 75252 Paris, France*

[2]*Sorbonne Universités, UPMC Université Paris 06, UMR7588 4 place Jussieu, 75252 Paris, France*

[3]*Laboratoire de Photonique et Nanostructures, CNRS, UPR 20, Route de Nozay, 91460 Marcoussis, France*

(Received 9 May 2014; revised manuscript received 7 July 2014; published 2 September 2014)

Surface acoustic waves (SAW) were generated on a thin layer of the ferromagnetic semiconductor (Ga,Mn)(As,P). The out-of-plane uniaxial magnetic anisotropy of this dilute magnetic semiconductor is very sensitive to the strain of the layer, making it an ideal test material for the dynamic control of magnetization via magnetostriction. The amplitude and phase of the transmitted SAW during magnetic field sweeps showed a clear resonant behavior at a field close to the one calculated to give a precession frequency equal to the SAW frequency. A resonance was observed from 5 to 85 K, just below the Curie temperature of the layer. A full analytical treatment of the coupled magnetization/acoustic dynamics showed that the magnetostrictive coupling modifies the elastic constants of the material and accordingly the wave-vector solution to the elastic wave equation. The shape and position of the resonance were well reproduced by the calculations, in particular the fact that velocity (phase) variations resonated at lower fields than the acoustic attenuation variations. We suggest one reinterpret SAW-driven ferromagnetic resonance as a form of resonant, dynamic, delta-E effect, a concept usually reserved for static magnetoelastic phenomena.

DOI: 10.1103/PhysRevB.90.094401 PACS number(s): 72.55.+s, 75.78.−n, 75.50.Pp, 62.65.+k

I. INTRODUCTION

Magnetostriction is the interaction between strain and magnetization, which leads to a change in a magnetic sample's shape when its magnetization is modified [1]. The opposite effect, inverse magnetostriction, whereby magnetization can be changed upon application of a strain, is particularly relevant to magnetic data storage technologies as a possible route towards induction-free data manipulation when used dynamically. It has been proposed for magnetization switching through resonant [2,3] or nonresonant processes [4,5], the latter possibly at play in early results of surface acoustic wave (SAW)-induced lowering of coercivity in Galfenol films [6]. In the case of precessional (resonant) switching, two features are necessary: sizable magnetoacoustic coupling (to trigger precession), and a highly nonlinear system (to force wide, noncircular precession needed for magnetization reversal). The first point has already been addressed in ferromagnetic metals, since the 1960s by ac electrical excitation of strain waves [7–12], and more recently by optical excitation of acoustic pulses [13,14]. The electrical approach consists in the radio-frequency (rf) excitation of a piezoelectric emitter. Using this technique, the triggering of magnetization precession by surface or bulk acoustic waves (BAWs) has been extensively studied in Ni-based films. Elegant data has also been obtained more recently on yttrium iron garnet, where BAWs were used to build a magnetic field tunable acoustic resonator [12].

In this work, we evidence magnetoacoustic coupling in a different type of material, a dilute ferromagnetic semiconductor (DFS). The low Curie temperature (100–180 K) of these compounds makes applications somewhat remote for now, but their magnetization precession frequencies are close to accessible SAW frequencies (GHz) and their small and tunable magnetic anisotropy make them good candidates to test SAW-assisted magnetization switching [2]. Moreover thanks to the semiconducting nature of host lattice [15,16], their magnetic properties can easily be band engineered and their magnetostrictive coefficients vary strongly with temperature, making them a good test-bench material to develop and validate theoretical models.

In this paper, we show experimental evidence of SAW-driven ferromagnetic resonance in a thin film of DFS, in our case (Ga,Mn)(As,P). Both acoustic attenuation and velocity variations are monitored in the time domain. Our experimental approach differs from previous work on metals in that we mainly use the temperature dependence of the effect to prove its resonant nature, as opposed to using different geometrical configurations (angle between magnetic field and SAW wave vector [9,11]). We solve the coupled magnetization and elastic dynamics equations and determine with a good match to the experimental data (Sec. IV) the expected resonance fields versus temperature and acoustic resonance shape. Here our main addition to the existing theoretical literature on the topic is to derive the form of a depth-decaying SAW traveling on the surface of a *cubic* medium, and to conclude on a very explicit dependence of the elastic constants on magnetization orientation and magnetoelastic coefficients. This ultimately leads us to reinterpret SAW-driven ferromagnetic resonance (FMR) as a form of resonant, dynamic, delta-E effect, a concept usually reserved for static magnetoelastic phenomena [17].

II. EXPERIMENTAL METHODS

A $d = 50$-nm-thick layer of $(Ga_{1-x},Mn_x)(As_{1-y},P_y)$ was grown by molecular beam epitaxy. After a $1h/250\,^{\circ}C$ anneal, its Curie temperature reached $T_c = 105$ K and its active Mn concentration $x^{\text{eff}} \approx 3.5\%$. Since GaAs is only weakly piezoelectric, a 70/250 nm bilayer of SiO_2/ZnO was sputtered onto the magnetic layer. Care was taken to keep the substrate

*thevenard@insp.jussieu.fr

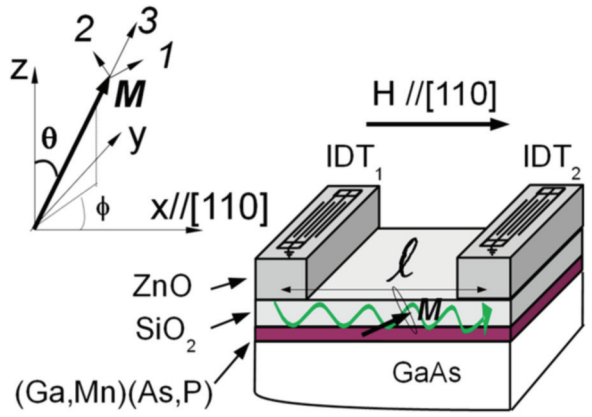

FIG. 1. (Color online) Structure of the sample (not to scale). 50 nm ferromagnetic epilayer, 70 nm SiO_2 buffer, and 250 nm piezoelectric ZnO. The IDTs have an aperture of 1 mm and are separated by 2 mm, but the effective length of the delay line is taken center to center of the IDTs, i.e., $l = 2.3$ mm. Upper left: Definition of the (x,y,z) and $(1,2,3)$ reference frames.

holder at relatively low temperature (150 °C) during the ZnO deposition so as to not further anneal the magnetic layer. The phosphorus ($y \approx 4\%$) was necessary to induce tensile strain in the layer, in order to obtain a dominantly uniaxial magnetic anisotropy [16,18], spontaneously aligning the magnetization perpendicular to plane. The resulting lattice mismatch of the layer to the substrate was of -0.161%.

Cr/Au interdigitated transducers (60 pairs of fingers, thickness 10/80 nm) were then evaporated and a window opened in the ZnO layer between the two IDTs (Fig. 1). The emitter (IDT_1) was excited by 550 ns bursts of rf voltage modulated at 1 kHz. After propagation along the [110] direction, the SAW was detected by the receiver IDT_2 and the signal was acquired with a digital oscilloscope over typically 4000 averages. This time-domain technique allowed us to (i) verify that the SAWs were indeed generated/detected in the sample, and (ii) clearly separate the antennalike radiation of IDT_1 (traveling at the speed of light), from the acoustic echo (traveling at the Rayleigh velocity), as shown in Fig. 2(a). The transit time lies around $\tau = 693$ ns, which immediately gives an experimental estimation of the Rayleigh velocity $V_r \approx 2886$ m s^{-1}. The transfer function of the device exhibited the typical band-pass behavior centered at the 549 MHz resonance frequency. The

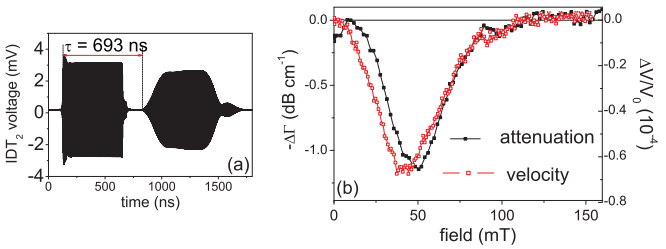

FIG. 2. (Color online) (a) Receiving IDT signal: The electromagnetic field radiated by the emitter is shortly followed by the transmitted surface acoustic wave. $T = 120$ K, 549 MHz. (b) Acoustic attenuation changes and relative velocity variations at $T = 80$ K. The opposite of $\Delta\Gamma$ has been plotted in order to highlight the different resonant field from the velocity variations.

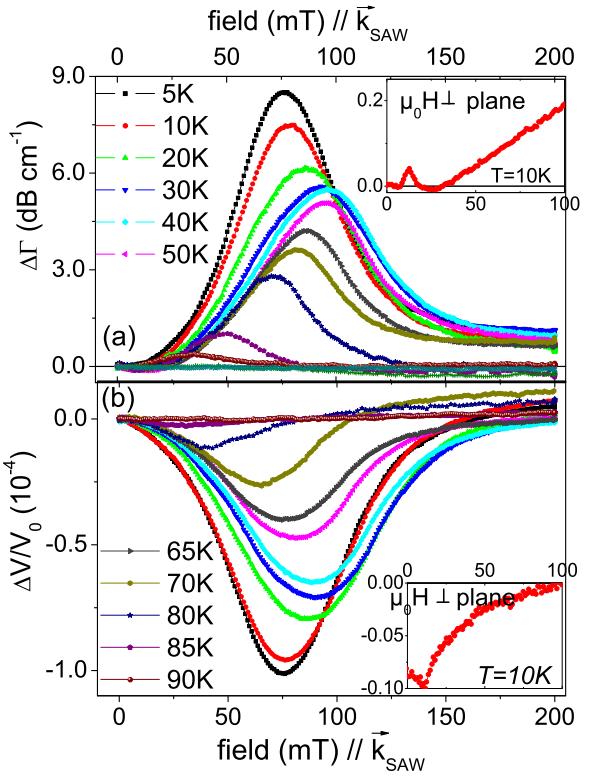

FIG. 3. (Color online) (a) Variation of acoustic attenuation and (b) relative velocity change of the SAW between 5 and 90 K for the field applied in plane, along the SAW wave vector. Insets: Field sweeps with the field applied perpendicular to plane at $T = 10$ K.

power applied to the IDT_1 was of +20 dBm (100 mW) on a 50 Ω load (30 dB conversion factor), resulting in an approximate strain [19] of $\varepsilon_{xx} \approx -2 \times 10^{-5}$ and $\varepsilon_{zz} \approx 6 \times 10^{-6}$. The excitation frequency was $\omega/2\pi = 549$ MHz, with the corresponding wavelength $\Lambda_{SAW} = 5\ \mu$m.

Unless specified, the field was applied in the plane of the sample, along the SAW wave vector, i.e., along a hard magnetic axis. A phase detection scheme then yielded the amplitude A and the phase $\phi = \omega\tau$ of the transmitted SAW. The phase variations $\Delta\phi$ were converted into relative velocity variations using $\Delta V/V_0 = \frac{\Delta\phi}{\omega\tau_0}$. The attenuation changes were computed using $\Delta\Gamma = -\frac{20}{l}\log\frac{A}{A_0}$. A_0 is an arbitrary reference amplitude. $l = 2.3$ mm and $\tau_0 = 797$ ns are the IDTs' center-to-center distance and the corresponding transit time.

III. EXPERIMENTAL RESULTS

A typical sweep at $T = 80$ K is shown in Fig. 2(b). Acoustic attenuation and velocity variations were both identical at low and high fields, but showed a clear feature at a particular field, hereafter called the resonance field. The resonance disappeared above 90 K. Measurements down to 5 K showed that the amplitude of the effect steadily increased with decreasing temperature (Fig. 3). The resonance field was not, however, monotonous with temperature, lying within 35–94 mT with a maximum at 30–40 K. The resonance width followed the same trend, within the bounds 9–17 mT. All curves shared the following features: a fairly symmetrical, nonhysteretic resonance, with the velocity variations systematically resonating

at a lower field than the amplitude variations. The maximum variation of acoustic attenuation, $\Delta\Gamma = 8.5$ dB cm^{-1} was observed at $T = 5$ K. It remains weak compared to the value of 200 dB cm^{-1} measured at 2.24 GHz on a similar device on nickel [10]. This is due to both the higher SAW frequency used by these authors, as the amplitude variations are directly proportional to ω (see Ref. [11], for instance), and the much lower magnetostrictive constants found in DFS. These are defined as the fractional change in sample length as the magnetization increases from zero to its saturation value and their maximum values lie around $|\lambda_{100}| \approx 9 \times 10^{-6}$ for (Ga,Mn)As [20] and $\lambda_{100} \approx 50 \times 10^{-6}$ for nickel [1].

IV. MODEL

We have shown above that at a particular applied field, the transmitted SAW was slightly absorbed (by a 19% decrease in amplitude at 5 K), and delayed (by about...90 ps) through its interaction with the magnetization of the (Ga,Mn)(As,P) layer. To confirm that this is indeed SAW-driven ferromagnetic resonance, we calculate the expected resonance fields and shapes. Microscopically, the resonance may be seen as the crossing of magnon and phonon dispersion curves at the wave vector imposed by the IDTs, k_{SAW}. Macroscopically, the total energy of the system may then be written [21] as the sum of a purely elastic contribution W, a purely magnetic energy (magnetocrystalline, demagnetizing, and Zeeman contributions, in units of field) F_{mc}, and the magnetostrictive contribution F_{ms}:

$$E_{\mathrm{tot}} = W + M_s F_{mc} + M_s F_{ms} \tag{1}$$

with

$$W = \frac{1}{2} c_{ijkl}\varepsilon_{ij}\varepsilon_{kl} = W_0 + W_{\mathrm{SAW}}(t), \tag{2}$$

$$F_{ms} = F_{ms,0} + F_{ms,\mathrm{SAW}} \tag{3}$$

$$= \left(\varepsilon_{zz} - \frac{\varepsilon_{xx}+\varepsilon_{yy}}{2}\right)\left[(A_{2\varepsilon}+A_{4\varepsilon})m_z^2 + \frac{A_{4\varepsilon}}{2}m_z^4 + A_{4\varepsilon}\left(m_x^4+m_y^4\right)\right], \tag{4}$$

$$F_{mc} = -\mu_0 \vec{H}.\vec{m} + \left[\frac{\mu_0 M_s}{2} - 3B_c\right]m_z^2 + \frac{5}{2}B_c m_z^4 - B_c\left(m_x^4+m_y^4\right) + \frac{B_{2\|}}{4}\left(m_x^2-m_y^2\right). \tag{5}$$

The components of the unit magnetization vector are defined as $m_i = M_i/M_s$ $(i = x,y,z)$ where M_s is the magnetization at saturation and $x \parallel [110]$. H is the applied field, B_c the cubic anisotropy constant, and $B_{2\|}$ the uniaxial one, distinguishing in-plane [110] and [1 −1 0] axes [22]. F_{ms} is the magnetoelastic contribution (in units of field) where the magnetostrictive coefficients $A_{2\varepsilon}, A_{4\varepsilon}$ depend on both the static strain felt by the layer $(\varepsilon_{xx,0},\varepsilon_{yy,0},\varepsilon_{zz,0})$, and the dynamic SAW-induced strain $[\varepsilon_{xx,\mathrm{SAW}}(t),\varepsilon_{zz,\mathrm{SAW}}(t)]$. The $\varepsilon_{xz,\mathrm{SAW}}(t)$ component of the SAW does not have any magnetostrictive action on the layer, and $\varepsilon_{yy,\mathrm{SAW}}(t)$ is not excited by our setup. The total strain components are thus given by $\varepsilon_{ii} = \varepsilon_{ii,0} + \varepsilon_{ii,\mathrm{SAW}}(t)$. At $T = 5$ K, the micromagnetic parameters are $A_{2\varepsilon} = 35$ T, $A_{4\varepsilon} = -5$ T, $B_c = -5$ mT, $B_{2\|} = -20$ mT, and $M_s = 36$ kA/m. At low temperature, $A_{2\varepsilon}$ is much bigger than $A_{4\varepsilon}$, so magnetostrictive terms in $A_{4\varepsilon}$ will first be neglected to ease the reading. The full derivation including $A_{4\varepsilon}$ is given in the Appendix, Sec. 5, and was used for the simulations shown in Figs. 4(b) and 5.

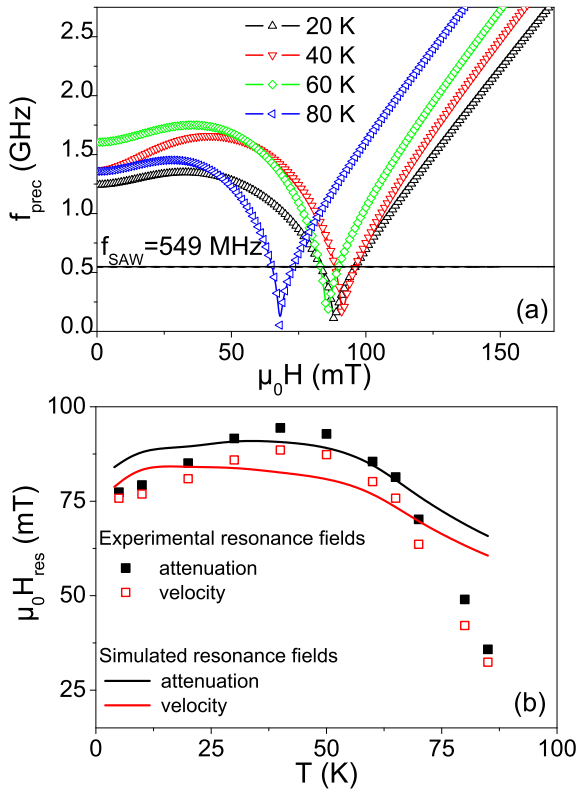

FIG. 4. (Color online) (a) Calculated precession frequency versus field applied along [110], no sample tilt. The horizontal line indicates the SAW frequency. (b) Measured (symbols) and simulated resonance fields (continuous line, sample tilt 1.2°, taking into account both $A_{2\varepsilon}$ and $A_{4\varepsilon}$) versus temperature for the attenuation (black) and velocity (red) variations.

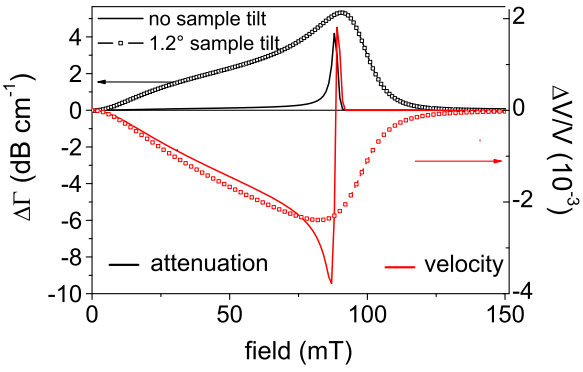

FIG. 5. (Color online) The variation of the acoustic attenuation (black) and relative variation of velocity (red) calculated with the $T = 40$ K micromagnetic parameters, $\alpha = 0.1$ and $F = 0.105$. The simulations were done taking into account both the $A_{2\varepsilon}$ and $A_{4\varepsilon}$ contributions, with (or without) a sample tilt in the (x,z) plane—symbols (full lines). The changes of attenuation and velocity without sample tilt have been divided by 20 for better visibility.

The magnetization and acoustics dynamics are then obtained by solving the Landau-Lifshitz Gilbert equation [Eq. (6)] and the elastic wave equation [EWE, Eq. (7)]. A similar procedure has been used by other authors [11,23,24] but our main interests here are to derive explicitly (i) the modification of the elastic constants under the influence of the magnetoelastic coupling and (ii) the form of the solution of a surface acoustic wave traveling on a *cubic* medium (which happens to be magnetostrictive).

$$\frac{\partial \vec{m}}{\partial t} = \frac{\gamma}{M_s}\vec{m} \times \vec{\nabla}_{\vec{m}} E_{\text{tot}} + \alpha \vec{m} \times \frac{\partial \vec{m}}{\partial t}, \tag{6}$$

$$\rho \frac{\partial^2 R_{\text{tot},i}}{\partial t^2} = \frac{\partial \sigma_{ik}}{\partial x_k} = \frac{\partial}{\partial x_k}\frac{\partial E_{\text{tot}}}{\partial \varepsilon_{ik}}. \tag{7}$$

α is an effective damping constant and γ the gyromagnetic factor. $\vec{m} = \vec{m_0} + \vec{m}(t)$ is the sum of the equilibrium magnetization unit vector and the rf magnetization and likewise for the displacement $\vec{R}_{\text{tot}} = \vec{R}_0 + \vec{u}(t)$. The displacements are related to the strain by $\varepsilon_{ij} = \frac{\partial R_{\text{tot},i}}{\partial x_j}$, ρ is the material density, and c_{ijkl} is the elastic constant tensor defined in the x,y,z frame (see Appendix, Sec. 2). Note that, as assumed by other authors [11,23] the exchange contribution was neglected in Eq. (6), as the typical SAW wave vector ($\approx 1/\Lambda_{\text{SAW}}$) is much smaller than the first spin-wave wave vector ($\approx 1/d$), leading to an essentially flat magnon dispersion curve for the frequencies considered here. For this reason, although we should in all rigor be talking about "spin-wave FMR," we will use the shorter term "ferromagnetic resonance."

We first briefly recall the derivation of the Polder susceptibility and of the precession frequency [25]. Following Dreher *et al.* [11], we define a second reference frame (1,2,3) where $\vec{m}_3$ is aligned with the static magnetization [polar coordinates (θ_0,ϕ_0); see Appendix, Sec. 1]. We are then left with two sets of unknowns: $(m_1,m_2)(t)$ (magnetization dynamics) and $(u_x,u_z)(t)$ (acoustic dynamics), as the transverse displacement u_y cannot be excited by our device. Solving Eq. (6) in the linear approximation with $m_i(x,t) = m_{0,i}e^{i(\Omega t - kx)}$ leads to the following system:

$$\begin{pmatrix} m_1 \\ m_2 \end{pmatrix} = [\chi]\begin{pmatrix} \mu_0 h_1 \\ \mu_0 h_2 \end{pmatrix}. \tag{8}$$

The dynamic fields are defined by $\mu_0 h_i = -\frac{\partial F_{ms,\text{SAW}}}{\partial m_i}|_{\vec{m}=\vec{m}_3}$. Neglecting the $A_{4\varepsilon}$ terms, the dynamic magnetoelastic energy then simply reads $F_{ms,\text{SAW}} = A_{2\varepsilon}\Delta\varepsilon(t)m_z^2$, so that $\mu_0 h_1 = A_{2\varepsilon}\Delta\varepsilon(t)(\cos^2\theta_0 - \sin 2\theta_0 m_1)$ and $\mu_0 h_2 = 0$. The susceptibility tensor $[\chi]$ (given in the Appendix, Sec. 1) depends on the static magnetic anisotropy constants, the damping and the SAW excitation frequency ω. Canceling the determinant of $[\chi]^{-1}$ yields the precession frequency (real part of Ω) $(\frac{\omega_{\text{prec}}}{\gamma})^2 = (F_{11} - F_{33})(F_{22} - F_{33}) - F_{12}^2$ where the terms F_{ij} stand for $\frac{\partial^2(F_{mc}+F_{ms,0})}{\partial m_i \partial m_j}$. Figure 4(a) shows the field dependence of this precession frequency at various temperatures, calculated from the FMR anisotropy coefficients. $f_{\text{prec}}(\mu_0 H)$ first decreases, crossing the SAW frequency of 549 MHz [full line in Fig. 4(a)] at a particular field. When the magnetization is aligned with the field (saturated), f_{prec} reaches a minimum. After saturation, the resonance frequency increases with field, and crosses f_{SAW} a second time. We will show below that this second crossing does not give rise to any magnetoacoustic resonance. The crossover fields of $f_{\text{prec}}(\mu_0 H)$ with f_{SAW} [Fig. 4(a)] can already give a good approximation of the expected resonance fields. It is not, however, sufficient to explain why the resonance fields are different for relative variations of the SAW attenuation and velocity. For this it is necessary to calculate how the SAW wave vector is modified by its interaction with the (Ga,Mn)(As,P) layer.

We place ourselves in the semi-infinite medium approximation and assume the SiO_2 layer to be a small perturbation to the system since its thickness is much smaller than Λ_{SAW} (see the Appendix, Sec. 3 for details on this point) so that the general form of displacement reads $u_\eta(x,t) = U_\eta e^{-\beta z}\exp[i(\omega t - kx)]$ $(\eta = x,y,z)$. This point differs from the infinite medium approach of Dreher *et al.* [11], which considers plane acoustic waves but does not take into account the z decay of the SAW, or the role of boundary conditions. Using the equilibrium conditions on the strain, the EWE [Eq. (7)] may be simplified into

$$\left[\rho\omega^2 + \left(\frac{A_\chi}{4} - c_{11}\right)k^2 + c_{44}\beta^2\right]u_x + \left(c_{44} + c_{13} + \frac{A_\chi}{2}\right)\beta i k u_z = 0, \tag{9}$$

$$\left(c_{44} + c_{13} + \frac{A_\chi}{2}\right)\beta i k u_x + \left[\rho\omega^2 + (c_{33} - A_\chi)\beta^2 - k^2 c_{44}\right]u_z = 0. \tag{10}$$

Note that here, we treat the case of a cubic lattice. This differs from most related work [11,23], where the isotropic approximation is kept, either because the material is polycrystalline, or to simplify calculations. In the above, we have introduced the complex constant:

$$A_\chi = M_s A_{2\varepsilon}^2 \sin^2(2\theta_0)\chi_{11}. \tag{11}$$

Two features come out. First, this system is the formal equivalent of the solution to the EWE in a cubic, nonmagnetostrictive material, with three of the elastic constants modified as follows:

$$\begin{aligned} c_{13} &\mapsto c'_{13} = c_{13} + A_\chi/2, \\ c_{11} &\mapsto c'_{11} = c_{11} - A_\chi/4, \\ c_{33} &\mapsto c'_{33} = c_{33} - A_\chi. \end{aligned} \tag{12}$$

The elastic constants are modified through A_χ which depends on the applied field, the anisotropy constants, and the SAW frequency (through χ_{11}). The real part of A_χ represents at most $\approx 10\%$ of the GaAs elastic constants. This parameter embodies the physics of the coupled magnon-phonon system as it modifies the elastic constants of the material. Equation (12), for instance, shows that the velocity of longitudinal phonons (proportional to $\sqrt{c'_{11}}$) is modified through the magnetoacoustic interaction.

The A_χ parameter cancels out when the material ceases to be magnetostrictive ($A_{2\varepsilon} = 0$) and/or when the magnetization is collinear or normal to the SAW wave vector. This is why no acoustic resonance is observed at the second crossing of $f_{\text{prec}}(\mu_0 H)$ with f_{SAW}, once the magnetization is aligned with

the applied field ($A_\chi|_{\theta_0=\pi/2}=0$). To check this point, we repeated the experiment with the field applied perpendicular to the sample (insets of Fig. 3). This time no resonance was observed, either in the attenuation changes or in the velocity variations. A small, hysteretic kink (return sweep not shown) was observed at a field coinciding with the coercive field of the layer, as already observed in Ref. [11]. This feature became undetectable above 20 K.

Secondly, using the full depth dependence of the displacements results in a coupling of the u_x and u_z components [β terms in Eqs. (9) and (10)], contrary to simpler cases treated previously [11]. In fact, it is through the z decay that c_{13} and c_{33} constants are modified by the magnetostrictive interaction; they would otherwise be left unchanged.

Canceling the determinant of Eqs. (9) and (10) yields two solutions with the corresponding absorption coefficients $\beta_{1,2}$ and x,z amplitude ratios $U_z/U_x=r_i$ ($i=1,2$; see Appendix, Sec. 4). As neither of these satisfy the normal boundary condition $\sigma_{xz}|_{z=0}=0$ at the vacuum interface, a linear combination of these two solutions needs to be considered:

$$u_x=[U_{x1}\exp(-\beta_1 z)+U_{x2}\exp(-\beta_2 z)]e^{i(\omega t-kx)}, \quad (13)$$

$$u_z=[U_{z1}\exp(-\beta_1 z)+U_{z2}\exp(-\beta_2 z)]e^{i(\omega t-kx)}. \quad (14)$$

The boundary conditions $\sigma_{xz}|_{z=0}=\sigma_{zz}|_{z=0}=0$ now lead to a new system, similar to Eqs. (9) and (10). Replacing r_i,β_i by their expressions and using $\omega/V_r=k$, its determinant eventually leads to Eq. (15).

$$\left(c_{44}-\rho\frac{\omega^2}{k^2}\right)\left[c'_{11}c'_{33}-c'^2_{13}-c'_{33}\rho\frac{\omega^2}{k^2}\right]^2 = c'_{33}c_{44}\left(c'_{11}-\rho\frac{\omega^2}{k^2}\right)\left(\rho\frac{\omega^2}{k^2}\right)^2. \quad (15)$$

This implicit polynomial equation in k may be solved numerically to yield the wave-vector solutions $k_{\rm sol}$ in the presence of magnetostrictive interaction. There are three distinct physical solutions to Eq. (15), but only the Rayleigh surface wave can be excited by our device [26]. In the absence of magnetostriction, the usual Rayleigh velocity [27] $V_r=\frac{\omega}{k_{\rm sol}|_{A_\chi=0}}=2852.2$ m s^{-1} is recovered, very close to the crude experimental estimation made earlier.

The amplitude of the transmitted SAW wave vector is proportional to $\exp[-{\rm Im}(k_{\rm sol})l]$, and its phase is equal to ${\rm Re}(k_{\rm sol})l$. The relative variations are calculated with respect to the zero-field values. We can now plot the expected relative variations of acoustic attenuation and velocity (e.g., at 40 K, Fig. 5) assuming we excite the IDTs at 549 MHz. In this calculation, we have also taken into account the $A_{4\varepsilon}$ term. The procedure is identical to the one described above, but the expressions are somewhat more cumbersome (see the Appendix, Sec. 5 for the corresponding effective elastic constants).

V. DISCUSSION

The variation of *attenuation* (Fig. 5, full black line) is monopolar and peaks at 88 mT, as expected from the simple crossing of $f_{\rm prec}(\mu_0 H)$ with $f_{\rm SAW}=\omega/2\pi$ (Fig. 4). The relative variation of *velocity* (full red line) is bipolar, and cancels out when the amplitude variation is maximum. Both curves are quite asymmetric, plummeting to zero when the magnetization is aligned with the field (92 mT). Introducing a small 1.2° sample tilt in the (x,z) plane with respect to the field direction pushes the saturation field away from the resonance field, restoring the symmetry of the resonance. This tilt may have been introduced when gluing the sample. It strongly reduces the magnitude of the effect, almost by a factor of 20. The attenuation resonance fields thus obtained are slightly higher than without tilt. The higher-field bump of the velocity variations disappears, making the resonance unipolar and at lower fields than the amplitude variations, as observed experimentally. It is interesting to compare these results to those of Dreher *et al.* [11], computed using a similar approach for an in-plane nickel thin film. Their closest comparable configuration is the one where the field is applied close to the sample normal (hard axis configuration). Their simulations (last line of Fig. 8 in Ref. [11]) also show that a bipolar shape is expected for the relative velocity, as the sample is excited closer and closer to its resonance frequency. Their experiments, however, also seem to show more of a monopolar behavior, for fields close to the sample normal.

Simulated attenuation and velocity variation resonance fields are now plotted along with the experimental ones in Fig. 4(b) as a function of temperature. Their values are well reproduced, and so is their nonmonotonous temperature variation. The latter can be traced back to a sign inversion of the $B_{2\parallel}$ term with temperature, i.e., a swap between [110] and [1 −1 0] easy axes around 40 K. At high temperature, the match is less good, the simulation overestimating the resonance fields. This may be the signature of a slight modification of the Curie temperature of the layer during the IDT deposition: The magnetostrictive coefficients would then fall off faster with temperature than those estimated by FMR before the IDT deposition. This could also account for the disappearing of the signal about 20 K below the Curie temperature (85 K, whereas $T_c=105$ K).

The resonance fields, as well as the fact that $\Delta V/V$ resonates at lower field than $\Delta\Gamma$ are overall well predicted. This is an indication that the data is reasonably well understood by our simple model. One of the results of this approach is that the elastic constants are modified resonantly via the magnetoacoustic coupling [Eq. (12)]. In this respect, we propose to reinterpret SAW-driven FMR as a resonant, dynamic form of the ΔE effect. This is a well-known effect [17,28] by which the Young modulus of a magnetostrictive material changes with applied field. Microscopically, the processes at play are generally the rotation of magnetization, often involving the rearrangement of magnetic domains. Although it is most often mentioned in static measurements [29], Ganguly *et al.* [23] had already identified the *dynamic* ΔE effect nature of the field-dependent velocity variations induced by a SAW on nickel. They had, however, demonstrated that it was a nonresonant effect. In the case of SAW-driven FMR, we suggest one interpret it as a *resonant* ΔE effect.

Let us briefly comment on the influence of the depth decay of the SAW on the interaction with the magnetization: As mentioned earlier, this resulted in a modification of, not only c_{11}, but also c_{13} and c_{33}. When not taken into account in the numerical calculation (e.g., at $T=40$ K), the peak of acoustic attenuation is found about 5 dB cm^{-1} lower than otherwise,

a sizable underestimation. The resonance field remains the same however, since c_{11}, c_{13}, and c_{33} are all linear in A_χ, whose resonance field is solely given by the micromagnetic parameters at the chosen temperature.

Finally, we wish to address the quantitative agreement between predicted and measured effects. The magnetostrictive constants had to be reduced by a filling factor F to best reproduce the amplitude of the effect since the magnetic layer occupies a small portion of the volume swept by the SAW: $A_{2\varepsilon} \mapsto FA_{2\varepsilon}$, $A_{4\varepsilon} \mapsto FA_{4\varepsilon}$. This effective medium approximation is routinely used in other solid state physics systems, such as the case of sparse quantum dots embedded in a waveguide [30]. We converged to a value of $F = 0.10$ to obtain good agreement between simulated and experimental attenuation variations. The simulated velocity variations are then, however, off by about an order of magnitude compared to the experiment (Fig. 5). This disparity in quantitative agreement between the experimental and simulated phase shift had already been observed in nickel [11]. We believe, however, that this filling factor has little physical meaning. First, we have shown that not only F, but also the sample tilt play a great role in the amplitude of the effect, and this value is not known experimentally. Secondly, the SAW amplitude is in fact not uniform across the depth Λ_{SAW}. To better reproduce quantitatively and qualitatively the shape and amplitude of the effect a more complete multilayer approach using a transfer matrix formalism would clearly need to be adopted, as was done, for instance, in Ref. [23].

VI. CONCLUSION

We have demonstrated the resonant excitation of magnetization precession in (Ga,Mn)(As,P) by a surface acoustic wave. Temperature-dependent measurements have clearly shown that the magnitude of the effect and the position of the resonance fields evolved together with temperature dependence of the magnetostrictive coefficients. An analytical description of a SAW traveling on a magnetostrictive cubic medium was derived. It was evidenced that in that case, the elastic tensor coefficients are modified by a complex value depending on the magnetostrictive coefficients, the SAW frequency, and the magnetization orientation (through the value of the applied field).

Two of these results—the first evidence of SAW-induced magnetoelastic in (Ga,Mn)(As,P) and the prediction of resonance fields—are important steps towards SAW-induced precessional magnetization switching in DFS. The generated strain ($\varepsilon_{\max} \approx 10^{-5}$) is for now about five times too small to obtain magnetization reversal, as sketched in the predictive diagram of Ref. [2]. This has been confirmed by the robust linearity of the observed effect versus acoustic power. The next step towards SAW-induced switching in DFS is therefore the optimization of the amplitude of the generated strain waves, paired with the elaboration of higher frequency combs, in order to work under smaller magnetic fields.

ACKNOWLEDGMENTS

This work was performed in the framework of the MANGAS and the SPINSAW projects (ANR 2010-BLANC-0424-02 and ANR 13-JS04-0001-01). We thank A. Lemaître (Laboratoire de Photonique et Nanostructures) for providing the (Ga,Mn)(As,P) sample, and M. Bernard (INSP) for helping us with the cryogenic setup.

APPENDIX

1. Magnetization dynamics

Following Dreher *et al.* [11], the (1,2,3) reference frame is defined by $\vec{m}_3$ being aligned with the magnetization equilibrium position (θ_0, ϕ_0) and the following correspondence:

$$\begin{aligned} m_x &= m_1 \cos\theta_0 \cos\varphi_0 - m_2 \sin\varphi_0 + m_3 \sin\theta_0 \cos\varphi_0, \\ m_y &= m_1 \cos\theta_0 \sin\varphi_0 + m_2 \cos\varphi_0 + m_3 \sin\theta_0 \sin\varphi_0, \\ m_z &= -m_1 \sin\theta_0 + m_3 \cos\theta_0. \end{aligned} \tag{A1}$$

The susceptibility tensor defined in Eq. (8) is given by

$$[\chi] = \frac{1}{D} \begin{pmatrix} F_{22} - F_{33} + \frac{i\alpha\omega}{\gamma} & -\left(F_{12} - \frac{i\omega}{\gamma}\right) \\ -\left(F_{12} + \frac{i\omega}{\gamma}\right) & F_{11} - F_{33} + \frac{i\alpha\omega}{\gamma} \end{pmatrix}, \tag{A2}$$

where $F_{ij} = \frac{\partial^2 (F_{mc} + F_{ms,0})}{\partial m_i \partial m_j}$ and

$$D = \left(F_{11} - F_{33} + \frac{i\alpha\omega}{\gamma}\right)\left(F_{22} - F_{33} + \frac{i\alpha\omega}{\gamma}\right) - F_{12}^2 - \left(\frac{\omega}{\gamma}\right)^2.$$

2. Elastic coefficient tensor

The elastic coefficient tensor being defined in the reference frame of a cubic material, we must rotate it by $\pi/4$ for the particular case of a SAW traveling along [110]. The equivalence with the usual elastic constants [27] C_{ij}^0 is

$$\begin{aligned} c_{11} &= \tfrac{1}{2} C_{11}^0 + \tfrac{1}{2} C_{12}^0 + C_{44}^0, \\ c_{12} &= \tfrac{1}{2} C_{11}^0 + \tfrac{1}{2} C_{12}^0 - C_{44}^0, \\ c_{13} &= C_{12}^0, \\ c_{33} &= C_{11}^0, \\ c_{44} &= C_{44}^0, \\ c_{66} &= \tfrac{1}{2} C_{11}^0 - \tfrac{1}{2} C_{12}^0. \end{aligned} \tag{A3}$$

Temperature variations of the elastic tensor have been neglected and (Ga,Mn)(As,P) elastic constants were assumed equal to those of GaAs. Note that since the medium is cubic, and not isotropic, the relationship $C_{12}^0 = C_{11}^0 - 2C_{44}^0$ is not verified.

3. Influence of the SiO_2/ZnO on the (Ga,Mn)(As,P) static strain

Although GaAs is naturally piezoelectric, a SiO_2/ZnO bilayer was sputtered onto the magnetic layer to increase the amplitude of the SAW-generated strain. The silica underlayer was required for good adhesion. An important question is whether the high temperature (150 °C) deposition of the SiO_2/ZnO bilayer modifies the magnetic layer's static strain. To check this, we performed room temperature high resolution x-ray rocking curves around the (004) reflection at different

steps of the bilayer deposition. The lattice mismatch of the reference (unpatterned) (Ga,Mn)(As,P) layer was around −0.152%, i.e., under tensile strain on GaAs. After the SiO_2 deposition, the lattice mismatch dropped to −0.136%. However, the lattice mismatch of the layer after deposition of the full SiO_2/ZnO stack returned close to the reference value, around −0.161%, and remained unchanged after removal of the ZnO layer. The rocking curves also pointed to the presence of a strain gradient extending into the GaAs substrate subsequently to the SiO_2/ZnO deposition. Given that the static strain of the magnetic layer seems to be affected by SiO_2/ZnO deposition, the FMR measurements of the magnetic anisotropy constants were done on the (Ga,Mn)(As,P)/SiO_2/ZnO stack after removal of the ZnO. We then used these values and the x-ray-diffraction-determined static strain to obtain the magnetostrictive coefficients of the layer, using the formulas given in Appendix A of Ref. [2].

4. Elastic wave equation

This paragraph details solutions to the elastic wave equation when taking the displacement as $u_\eta = U_\eta e^{-\beta z}\exp[i(\omega t - kx)]$ ($\eta = x,y,z$). Inserting this expression into Eq. (7) leads to the system of Eqs. (9) and (10). Canceling this determinant leads to the following bisquared equation in $q = \beta/k$ using the effective elastic tensor coefficients defined in Eq. (12):

$$q^4 + \frac{\left[-c_{44}^2 - c'_{11}c'_{33} + (c'_{13}+c_{44})^2\right] + \rho V_r^2(c'_{33}+c_{44})}{c'_{33}c_{44}}q^2 + \frac{\left(c'_{11}-\rho V_r^2\right)\left(c_{44}-\rho V_r^2\right)}{c'_{33}c_{44}} = 0. \tag{A4}$$

This equation has two physical solutions, $q_i = \beta_i/k$ with $U_z/U_x = r_i$ ($i = 1,2$) that verify

$$q_1^2 + q_2^2 = \frac{\left[c_{44}^2 + c'_{11}c'_{33} - (c'_{13}+c_{44})^2\right] - \rho V_r^2(c'_{33}+c_{44})}{c'_{33}c_{44}}, \tag{A5}$$

$$q_1^2 q_2^2 = \frac{\left(c'_{11}-\rho V_r^2\right)\left(c_{44}-\rho V_r^2\right)}{c'_{33}c_{44}}, \tag{A6}$$

$$r_{1,2} = \frac{i\beta_{1,2}k(c'_{13}+c_{44})}{k^2 c_{44} - \beta_{1,2}^2 c'_{33} - \rho\omega^2}. \tag{A7}$$

As neither of these satisfy the normal boundary condition $\sigma_{xz}|_{z=0} = 0$ at the vacuum interface, a linear combination of these two solutions needs to be considered, as further developed in the text.

5. Solutions when taking into account the $A_{4\varepsilon}$ term

At high temperatures ($T \geqslant T_c/2$), $A_{4\varepsilon}$ (cubic anisotropy) is routinely 10 smaller than $A_{2\varepsilon}$ (uniaxial anisotropy). At lower temperatures, we rather have $A_{2\varepsilon} \approx 4$–$5A_{2\varepsilon}$. Following the same calculation as in the text but taking into account $A_{4\varepsilon}$ gives the following modified elastic constants:

$$\begin{aligned} c_{13} &\mapsto c'_{13} = c_{13} + A_\xi DB, \\ c_{11} &\mapsto c'_{11} = c_{11} - A_\xi D^2, \\ c_{33} &\mapsto c'_{33} = c_{33} - A_\xi B^2, \end{aligned} \tag{A8}$$

where the field is applied along a [±110] axis and

$$\begin{aligned} A_\xi &= M_s \sin^2(2\theta_0)\chi_{11}, \\ B &= A_{2\varepsilon} + \frac{A_{4\varepsilon}}{2}\left[1 + 3\cos(2\theta_0)\right], \\ D &= B/2. \end{aligned} \tag{A9}$$

The shape and position of the resonance remain globally unchanged, but the amplitude of the effect (on both the relative attenuation and the velocity variations) is strongly diminished.

[1] E. du Tremolet de la Lacheisserie, *Magnetism: Fundamentals*, 1st ed. (Springer, New York, 2006).

[2] L. Thevenard, J.-Y. Duquesne, E. Peronne, H. J. von Bardeleben, H. Jaffres, S. Ruttala, J.-M. George, A. Lemaître, and C. Gourdon, Phys. Rev. B **87**, 144402 (2013).

[3] O. Kovalenko, T. Pezeril, and V. V. Temnov, Phys. Rev. Lett. **110**, 266602 (2013).

[4] W. Li, P. Dhagat, and A. Jander, IEEE Trans. Magn. **48**, 4100 (2012).

[5] S. Davis, A. Baruth, and S. Adenwalla, Appl. Phys. Lett. **97**, 232507 (2010).

[6] W. Li, B. Buford, A. Jander, and P. Dhagat, IEEE Trans. Magn. **50**, 37 (2014).

[7] M. Pomerantz, Phys. Rev. Lett. **7**, 312 (1961).

[8] H. Bömmel and K. Dransfeld, Phys. Rev. Lett. **3**, 83 (1959).

[9] I.-a. Feng, M. Tachiki, C. Krischer, and M. Levy, J. Appl. Phys. **53**, 177 (1982).

[10] M. Weiler, L. Dreher, C. Heeg, H. Huebl, R. Gross, M. S. Brandt, and S. T. B. Goennenwein, Phys. Rev. Lett. **106**, 117601 (2011).

[11] L. Dreher, M. Weiler, M. Pernpeintner, H. Huebl, R. Gross, M. S. Brandt, and S. T. B. Goennenwein, Phys. Rev. B **86**, 134415 (2012).

[12] N. I. Polzikova, A. O. Raevskii, and A. S. Goremykina, J. Commun. Technol. Electron. **58**, 87 (2013).

[13] J.-W. Kim, M. Vomir, and J.-Y. Bigot, Phys. Rev. Lett. **109**, 166601 (2012).

[14] M. Bombeck, A. S. Salasyuk, B. A. Glavin, A. V. Scherbakov, C. Brüggemann, D. R. Yakovlev, V. F. Sapega, X. Liu, J. K. Furdyna, A. V. Akimov, and M. Bayer, Phys. Rev. B **85**, 195324 (2012).

[15] T. Dietl, H. Ohno, and F. Matsukura, Phys. Rev. B **63**, 195205 (2001).
[16] M. Cubukcu, H. J. von Bardeleben, K. Khazen, J. L. Cantin, O. Mauguin, L. Largeau, and A. Lemaître, Phys. Rev. B **81**, 041202(R) (2010).
[17] E. Lee, Rep. Progr. Phys. **18**, 184 (1955).
[18] A. Lemaître, A. Miard, L. Travers, O. Mauguin, L. Largeau, C. Gourdon, V. Jeudy, M. Tran, and J.-M. George, Appl. Phys. Lett. **93**, 021123 (2008).
[19] D. Royer and E. Dieulesaint, *Elastic Waves in Solids I: Free and Guided Propagation*, Advanced Texts in Physics (Springer, New York, 2000).
[20] S. C. Masmanidis, H. X. Tang, E. B. Myers, M. Li, K. DeGreve, G. Vermeulen, W. V. Roy, and M. L. Roukes, Phys. Rev. Lett. **95**, 187206 (2005).
[21] L. Landau, L. E. M, and L. Pitaevskii, *Electrodynamics of Continuous Media* (Elsevier, Butterworth-Heinemann, Amsterdam, 1984).
[22] This anisotropy has been attributed to the presence of a shear strain ϵ_{xy} in the [100] reference frame [Sawicki *et al.*, Phys. Rev. B **71**, 121302(R) (2005)], which would imply that the SAW could have an action on it. However, since no experimental evidence of this shear strain has ever been shown, we have not taken it into account.
[23] A. K. Ganguly, K. L. Davis, D. Webb, and C. Vittoria, J. Appl. Phys. **47**, 2696 (1976).
[24] N. Polzikova, S. Alekseev, I. Kotelyanskii, A. Raevskiy, and Y. Fetisov, J. Appl. Phys. **113**, 17C704 (2013).
[25] L. Baselgia, M. Warden, F. Waldner, S. L. Hutton, J. E. Drumheller, Y. Q. He, P. E. Wigen, and M. Maryško, Phys. Rev. B **38**, 2237 (1988).
[26] There are two other physical solutions. Each of them is the superposition of bulk quasilongitudinal and quasitransverse acoustic waves traveling away from the surface. These components cannot be excited simultaneously by our device because Bragg's condition cannot be fulfilled simultaneously for both components.
[27] R. I. Cottam and G. A. Saunders, J. Phys. C: Solid State Phys. **6**, 2105 (1973).
[28] K. Honda and T. Terada, Philos. Mag. **13**, 36 (1907).
[29] A. E. Clark, J. B. Restorff, M. Wun-Fogle, and J. F. Lindberg, J. Appl. Phys. **73**, 6150 (1993).
[30] R. Melet, V. Voliotis, A. Enderlin, D. Roditchev, X. L. Wang, T. Guillet, and R. Grousson, Phys. Rev. B **78**, 073301 (2008).